



Contents lists available at ScienceDirect

Quaternary Science Reviews

journal homepage: www.elsevier.com/locate/quascirev

A 550 ka record of aeolian activity near North West Cape, Australia: inferences from grain-size distributions and bulk chemistry of SE Indian Ocean deep-sea sediments

Jan-Berend W. Stuut^{a,b,*}, Felix Temmesfeld^a, Patrick De Deckker^c^a NIOZ – Royal Netherlands Institute for Sea Research, P.O. Box 59, 1790 AB Den Burg, The Netherlands^b MARUM – Center for Marine Environmental Sciences, Bremen University, 28359 Bremen, Germany^c Research School of Earth Sciences, The Australian National University, Canberra ACT 0200, Australia

ARTICLE INFO

Article history:

Received 24 June 2013

Received in revised form

26 October 2013

Accepted 1 November 2013

Available online 27 November 2013

Keywords:

Aeolian dust

Monsoon

End-member modelling

Grain size

XRF scan

Zr/Fe

Ti/Ca

ABSTRACT

The terrigenous fraction of sediments from a deep-sea sediment core recovered from the northwestern Western Australian continental slope offshore North West Cape, SE Indian Ocean, reveals a history of Western Australian climate throughout the last 550 ka. End-member modelling of a data set of grain-size distributions ($n = 438$) of the terrigenous sediment fraction allows to interpret the record in terms of aeolian and fluvial sediment deposition, both related to palaeo-environmental conditions in the North West Cape area. The data set can be best described by two aeolian end members and one fluvial one. Changes in the ratio of the two aeolian end members over the fluvial one are interpreted as aridity variations in northwestern Western Australia. These grain-size data are compared with bulk geochemical data obtained by XRF scans of the core. Log-ratios of the elements Zr/Fe and Ti/Ca, which indicate a terrigenous origin, corroborate the grain-size data. We postulate that the mid- to late Quaternary near North West Cape climate was relatively arid during the glacial and relatively humid during the interglacial stages, owing to meridional shifts in the atmospheric circulation system. Opposite to published palaeo-environmental records from the same latitude (20°S) offshore Chile and offshore Namibia, the Australian aridity record does not show the typical southern hemisphere climate variability of humid glacial and dry interglacials, which we interpret to be the result of the relatively large land mass of the Australian continent, which emphasises a strong monsoonal climatic system.

© 2013 Elsevier Ltd. All rights reserved.

1. Introduction

Terrigenous sediments deposited on the seafloor of a subtropical ocean are a mixture of a pelagic component brought in by wind and a hemipelagic component brought in by rivers and supplied from the shelf. In addition, downslope transport of shelf sediments may, at times, also occur as mass flows resulting in turbidites. Terrigenous sediments delivered to the ocean by rivers usually do not go further than the estuary, due to the sudden increase in accommodation space and the change of current velocity causing the coarser size fraction to rapidly settle on the sea floor. The portion of the fine-grained sediment that makes it to the continental slope, which is typically 4–6 μm (e.g., Prins et al., 1999, 2000, 2002; Stuut et al., 2002; Holz et al., 2004; Stuut et al., 2007) is mainly deposited on

the slope and rise, and can reach the deep basin by low-density turbidity currents and nepheloid-layer sedimentation. The flux of hemipelagic sediments that is associated with continental runoff can thus be used as a proxy for continental ‘humidity’ as an increase of fluvial sediments in deep-sea cores imply stronger river discharge to sea (Prins and Weltje, 1999; Stuut et al., 2002; Stuut and Lamy, 2004).

Aeolian sediments deposited in the deep sea close to the continent are definitely coarser grained than hemipelagic sediments (Koopmann, 1981; Sirocko et al., 1991; Stuut et al., 2002; Weltje and Prins, 2003; Stuut et al., 2005; McGee et al., 2013). For this reason, the fluvially-derived and aeolian sediment fractions are relatively easily distinguished in the mixture that deep-sea sediments comprise. In addition, the analysis of aeolian dust not only allows the estimation of aridity in the source regions through flux determinations, but also the intensity of the transporting winds through grain-size measurements of the dust fraction (Sarnthein et al., 1981; Rea, 1994; Stuut et al., 2002). Consequently, if the mixture of terrigenous sediments can be ‘unmixed’ on the basis of

* Corresponding author. NIOZ – Royal Netherlands Institute for Sea Research, P.O. Box 59, 1790 AB Den Burg, The Netherlands.

E-mail address: jbstuut@nioz.nl (J.-B.W. Stuut).

the grain-size distributions of the different components, it can be used to reconstruct changes in continental climate, especially for distinguishing humid from arid phases in the geologic record (e.g., [Montero-Serrano et al., 2010](#)).

In this study, we applied an inversion algorithm for end-member modelling of compositional data ([Weltje, 1997](#)) to the grain-size distributions of the terrigenous fraction from a sediment core from the northwest Australian continental slope. This method, developed for unmixing of multiple-sourced basin fills, is a powerful tool for the unmixing of grain-size distributions that are composed of sediment sub-populations, i.e. end members ([Prins and Weltje, 1999](#); [Stuut et al., 2002](#); [Weltje and Prins, 2003](#); [Stuut et al., 2006, 2007](#); [Weltje and Prins, 2007](#); [Tjallingii et al., 2008](#); [McGregor et al., 2009](#); [Filipsson et al., 2011](#); [McGee et al., 2013](#)). This sediment core was shown to register continuous sedimentation during the past 550 ka ([Spoonner et al., 2011](#)), and therefore offers the unique opportunity to study Australia's climate history over such a long period of time.

2. Australia's environmental history

2.1. Australia's past arid environments

As Australia is the driest inhabited continent on the planet, there has always been a lot of interest in its climate history. Since the first review of Australia's long-term environmental history by [Bowler \(1976\)](#), it has been hypothesised that Australia may have been a very dry place throughout geologic history, but that this is hard to verify as there are hardly any long continuous archives from which palaeo-environmental conditions can be reconstructed. Mostly from dune-field reconstructions and lake-level histories, [Bowler \(1976\)](#) concluded that Australia has been characterised by relatively arid glacials and wet interglacials probably since 300 ka BP. Due to dating issues he could only be certain about this climate pacing throughout the last 40 ka BP, which comes down to a maximum in aridity during the Last Glacial Maximum (=LGM) and somewhat wetter conditions before and after that period. The cause for this hydrological deficit would be increased by atmospheric circulation due to low sea levels during glacials and, as a consequence, reduced precipitation. [Bowler \(1976\)](#) argued that we should explore the marine sediment archive to find long continuous palaeo-climate records. Without showing any palaeo-environmental records, in his review of Quaternary aeolian dust processes and sediments in the Australian region, [McTainsh \(1989\)](#) argued that Late Pleistocene aridity rates of dust entrainment, transport and deposition were significantly higher than at present. However, he also argued that the major part of the dust was made available for transport at wet-to-dry conditions, and that some moisture is needed to create dust after all. Just like [Bowler \(1976\)](#), [McTainsh \(1989\)](#) also argued that the ocean sediments of the Tasman Sea, the Pacific and Indian Oceans would have received massive amounts of aeolian sediment. See [Thiede \(1979\)](#) for the Tasman Sea.

[De Deckker et al. \(1991\)](#) published a 30 ka record of aeolian deposition in the Gulf of Carpentaria by studying quartz grains >60 µm. From this record, they derive a cyclic occurrence of increased aridity, occurring every 2.25 ka. Already in 1979, [Thiede](#) examined the distribution of aeolian quartz in the Tasman Sea which indicated a supply of material originating from the Australian landmass and that coincided with the major wind/dust plume offshore eastern Australia which [Bowler](#) had defined in his 1976 paper. [Hesse \(1994\)](#) subsequently studied a number of sediment cores from the Tasman Sea and applied the method that [Rea and Janecek \(1981\)](#) had developed to extract the aeolian fraction from distal marine sediments. The method includes several chemical

treatment steps to remove marine organic matter as well as sieving over a 63 µm sieve to remove coarse radiolarian and volcanic components. Most likely, in the process a large share of the fraction of interest, which we now know is relatively coarse grained so close to the source, was also sieved off. Mass-accumulation rates of the terrigenous fraction, which was thought to completely consist of wind-blown dust, were calculated. We now know that this size fraction of deep-sea sediments that are deposited close to the continent contains a large share of fluvially transported material (e.g., [Prins and Weltje, 1999](#); [Stuut et al., 2002](#); [Weltje and Prins, 2003](#); [Stuut and Lamy, 2004](#); [Stuut et al., 2005, 2007](#); [Mulitza et al., 2008](#); [Meyer et al., 2013](#)), and that [Rea and Janecek's](#) method only applies to the distal parts of the ocean. Nonetheless, [Hesse \(1994\)](#) provided a reconstruction of the zonal movements of the so-called Southeast dust plume, which presently lies at about 33°S, and which migrated North by about 3° latitude during glacial times. Roughly, glacial–interglacial swings could be recognised in the transect of Tasman Sea cores, with dust fluxes increasing about three fold during glacial stages. [Hesse \(1994\)](#) further hypothesised that there clearly is a record of long-term increase in dust flux from Australia, beginning probably in Stage 10, some 350 ka BP ago, marking the onset of aeolian activity in the interior of southeastern Australia. This marks the transition to true aridity in this area following a gradual continent-wide drying since the Miocene ([Bowler, 1976](#)).

With the development of luminescence methods, absolute dating of dune deposits became possible, and this led [Hesse and McTainsh \(2003\)](#) to publish a new review on Australian dust deposits, modern processes and the Quaternary record. In this review, these authors compare modern dust processes and past dust deposits all through the Australian continent, from which they conclude that the marine record of dust flux (in the Tasman Sea) during the LGM shows at least a threefold increase in dust flux, compared with the Holocene, driven by weakened Australian monsoon rains and drier westerly circulation. Finally, also [Hesse and McTainsh \(2003\)](#) conclude that there is an urgent need for well-dated and quantified records of palaeo-environmental change in Australia.

2.2. Australia's North West Cape – dunes and rivers

North West Cape occurs at the northwest tip of Western Australia and forms a peninsula which is commonly referred to as Cape Range or Northwest Cape. It straddles the northern limit of the arid tropics. It is just north of North West Cape that a portion of the Leeuwin Current (LC) veers to the south to commence its journey along the western coast of Western Australia ([Fig. 1B](#)). Another portion of the LC continues straight into the central Indian Ocean. It is accepted that during the Last Glacial, the largest component of the LC followed that path ([Gingele et al., 2001](#)).

Cape Range is bordered to the west by Ningaloo Reef and Exmouth Gulf to the east. It is characterised by a fairly high relief which is incised by a number of small rivers, but there is evidence that strong fluvial discharge regimes must exist at times since those streams host a large amount of gravel and boulders and their gullies are several metres high. The relief of Cape Range reaches well over 300 m and is besieged also by extensive longitudinal dune fields which vary in direction [from NNW at the bottom western corner of the Cape, to NNE on its eastern side adjacent to Exmouth Gulf]. Some dunes can frequently reach heights of well over 10 m, but further south, east of Carnarvon where the Gascoyne River ([Fig. 1](#)) reaches the sea, in the Kennedy Range, dunes can reach up to 20 m and have an almost east west direction. We have sampled some of these dunes on either sides of Cape Range and found an extensive variety of dunes with significant colour differences – on the

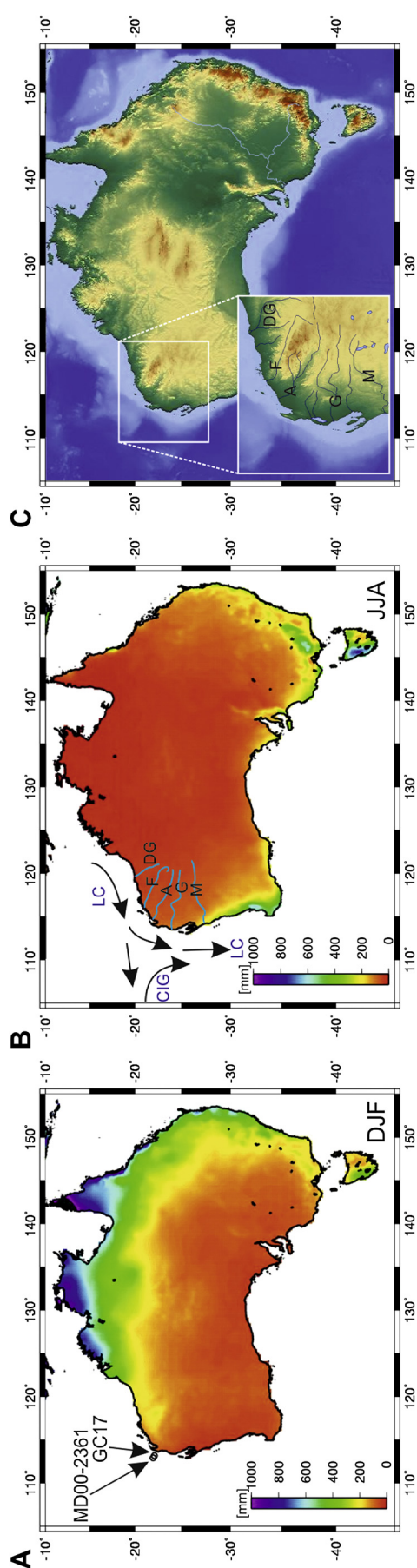


Fig. 1. Rainfall maps of Australia for austral summer (A: December to February; DJF) and austral winter (B: June to August; JJA), illustrating the sharp contrast in rainfall between the seasons. The core sites on the continental shelf offshore North West Cape are indicated in A. The general oceanographic setting is indicated in B, with the Leeuwin Current (LC), and Central Indian Gyre (CIG), and Central Indian Gyre (CIG), and Central Indian Gyre (CIG). The major rivers of northwestern Western Australia are indicated in B and C. De Grey (DG), Fortescue (F), Ashburton (A), Gascoyne which meets the ocean at Carnarvon (C) and Murchison (M). The two rainfall maps were generated by P. Wintersteller (MARUM) using Generic Mapping Tool (GMT), based on re-analysed global precipitation data between 1961 and 1990 (New et al., 2002). The topographical map was created using www.maps-for-free.com.

Munsell Colour Chart – dark red brown [10R 3/6], dull reddish brown [10R 4/4], dull yellow orange [10YR 7/4], very dark reddish brown [2.5 2/2] to dull orange [5YR 6/3], but all consistently made of quartz stained in the colours mentioned herewith.

There are also several important rivers that border the north-west shelf of Western Australia and the western side of West Cape and further south. The Fortescue River (Fig. 1), for example, is some 760 km long, its headwaters lie at 600 m above sea level and has a catchment of $49.5 \cdot 10^3$ km². (<http://www.water.gov.au/RegionalWaterResourcesAssessments>). Its mean annual flow is 391 GL [see further discussion in Section 7].

Concerning the Gascoyne River, which flows north of Shark Bay, it is 760 km long, its source lies at 514 m above sea level and has a catchment of $68.7 \cdot 10^3$ km² (Dodson, 2009). The latest extreme event during which cyclone Steve affected the region, saw the flow of the river near Carnarvon (at Nine Mile Bridge) reaching a value 3104 GL in January 2000 (Dodson, 2009). For more details on Cape Range, refer to Humphreys (1993).

3. Present-day setting, climatology, and oceanography

3.1. Land-desert fringe

The Australian arid zone occupies much of the continent, except the coastal fringe (Fig. 1). It is a classical sub-tropical desert lying underneath the descending limb of the southern hemisphere Hadley cell. As there are hardly any major topographic barriers, it responds to seasonal movement of the zonal circulation features and this movement defines the variable character of the arid zone over this large continent. Northern Australia experiences a mild dry winter with southeasterly trade winds of moderate strength. Moisture is principally brought to northern Australia by the summer monsoon. These rains penetrate to at least the tropics and frequently further south, associated with low pressure troughs and cyclones (Hesse et al., 2004).

3.2. Rivers

Today, there are no active, permanent major river systems on the northwestern part of the Australian continent, although the present-day topography clearly indicates that there have been such major river systems in the past (Vörösmarty et al., 2000). Considering the combination of the arid conditions in the area and the strongly seasonal character of (heavy) rains, it is not hard to imagine that surface erosion by these river systems must have been immense and hence, also fluvial sediment supply to the ocean must have been extensive.

3.3. Seasonality

There are clear differences today between patterns of rainfall along the northwestern coast of Western Australia. In the north around 22°S, predominant rains occur during 2 periods [February–March] and [May–June] – ignoring cyclones – and the rest of the year is characterised by the dry period [data obtained from www.bom.gov.au]. Further South, like for Carnarvon [24° 50'S] where the Gascoyne River discharges, the predominant rains occur in May to August.

3.4. Cyclones, resulting in extensive river discharge

Significant amounts of rain can fall during periods of cyclonic activity and the northern coast of Australia [and eventually inland when cyclonic depression continue along their paths] is well known for being affected by several cyclones every year. Heavy rains can produce massive floods and discharge from rivers into the

ocean. The northern coast of Western Australia is particularly prone to cyclones. For example, in 1997, the Ashburton River recorded a flow of 4.5 GL/yr compared to an average of 0.5 GL/yr for the period of 1982–1994 (Leighton and Mitchell, 1997). The flooding in 1997 occurred during a slow moving pressure system formed near Broome to the east, and some 477 mm rained in 24 h at Onslow near the mouth of the river.

3.5. Leeuwin Current, coastal currents

A very characteristic and well-studied phenomenon of the southeastern Indian Ocean is the Leeuwin Current (see Spooner et al., 2011 for more details). Compared to other locations in the southern hemisphere, the Leeuwin Current is an anomalous eastern boundary current transporting southward warm, low salinity water formed within the Indonesian Throughflow and the Central Indian Gyre (Spooner et al., 2011). The influence of this current extends offshore Western Australia from North West Cape in the north down to Cape Leeuwin at the south-western tip of Western Australia and it can, at times, extend as far as the west coast of Tasmania (see De Deckker et al., 2012). The Leeuwin Current is seasonal, being more predominant during the Austral winter and has a temporal variability due to variation in the alongshore pressure gradient and prevailing equatorward winds. It is also strongly influenced by ENSO (El Niño Southern Oscillation) being strengthened during La Niña years and weaker during El Niño years.

4. Previous work done on core MD00-2361

Based on planktonic foraminifera assemblages, sea-surface temperature estimates reconstructed from those assemblages, together with the $\delta^{18}\text{O}$ and $\delta^{13}\text{C}$ signals of near-surface dwelling foraminifera (*Globigerinoides ruber*), Spooner et al. (2011) reconstructed the vertical structure of the water column offshore Western Cape for the past 550 ka. They concluded that the Leeuwin Current was present along the western coastline of Australia even during glacial periods. During those times, there was a greater influence of South Indian Subtropical Water (STW) and South Indian Central Water (SICW) due to a 3–4° northward migration of the Indonesian Throughflow Water/South Indian Central Water frontal system. This resulted in an overall 6–9 °C decrease in SST, paralleled by a thickening and greater homogeneity of the mixed layer. The increased influence of STW and SICW also suggests that the West Australian Current, which presently sits below the Leeuwin Current, was strengthened during the glacial periods and contributed to a weakening of the Leeuwin Current. Conversely, the Leeuwin Current was 'stronger' during interglacial periods due to a thicker component of Indonesian Throughflow Water sourced from the Indo Pacific Warm Pool.

Several investigations have already been carried out on a much shorter deep-sea core (Fr10/95-GC17) located some 50 km to the SE of core MD00-2361. Its exact location is 22° 02.74'S 113° 30.11'E and was taken at 1093 m water depth, Fig. 1. Of relevance to this study is the optical dating of quartz grains taken from 7 different horizons in that core, further indicating the presence of aeolian quartz in layers that would have been deposited during MIS 3–1 (Olley et al., 2004). These dates were compared against AMS¹⁴C dates obtained from the same core for 15 intervals (Olley et al., 2004; van der Kaars et al., 2006). The work by Gingele et al. (2001) and Ehlert et al. (2011) on clays extracted from the same core identifies an increase in the percentage of illite clays at around 15.5 ka, from ~30% for the LGM and a bit after that, to well over 35–40% since then, and well into the Holocene. Gingele et al. (2001) noted that this shift to higher values of illite is interpreted

to a much more extensive contribution of a fluvial load from large rivers such as the Ashburton River, located east of West Cape, and the Gascoyne River south of West Cape (Fig. 1). The latter fluvial sediments would have been brought to the core site by the Ningaloo Current (NC, see Taylor and Pearce, 1999, Woo et al., 2006), whereas the Ashburton-derived fluvial clays would have been brought by the Leeuwin Current. We note that today the NC is strongest from September to April [austral spring and summer], whereas the LC flows all year round offshore northwestern Australia, but is particularly strong in winter along the west coast of Australia and more so under a La Niña mode. Hence, we believe that if the Gascoyne River did flow in summer [as would be expected under a strong monsoonal system], some of its fluvial sediments in suspension could be easily transported [and deposited] to the coring site. As the LC does flow all year round along the north-western coast of Australia, sediment from the Ashburton River could also eventually settle at the core site. Under a glacial scenario, the monsoonal system would have disappeared (see De Deckker et al., 2002 for justification), so little water would have flowed from the rivers mentioned above, and therefore no or little fluvial sediments would have reached the core site.

In addition, Gingele et al. (2001)'s investigation on the clay-silt ratio done on the same core points to a coarser terrigenous fraction during the glacial phase, which these authors implied for a drier climate in the Western Australian source area, viz. desert dunes, some of which are amazingly close to the coast (<10 km) and would even have extended on the exposed shelf during the period of low sea level.

The palynological investigations carried out on core Fr10/95-GC17 by van der Kaars and De Deckker (2002) and van der Kaars et al. (2006) clearly confirm Gingele et al. (2001)'s interpretation: at the LGM, the mean annual rainfall (estimated from the pollen evidence to be ~300 mm/year, whereas in the early Holocene, this value had increased to ~500 mm/year. The postglacial rainfall increasing mostly in the summer (as a consequence of a return of a monsoonal system) to the detriment of winter values. The drier glacial saw high percentages of Asteracea Tubuliflorae, Chenopodiaceae/Amaranthaceae and *Callitris* values (van der Kaars and De Deckker, 2002). This coincided with a low pollen flux which provides additional evidence for drier conditions (van der Kaars and De Deckker, 2002) despite the fact that the core sites would have been nearer to the exposed shelf. Thus, a reduced vegetation cover would have helped towards the mobility of aeolian dunes in the region.

5. Materials and methods

5.1. Stratigraphy

Piston core MD00-2361 was recovered from the continental slope offshore North West Cape of Western Australian at 22°04.92'S/113°28.63'E at 1805 m water depth (Fig. 1). The sediment core's total length is 42 m. The upper 13.5 m of this core was studied by Spooner et al. (2011) and their age model shows that this portion contains a record of about 550 ka.

5.2. XRF analyses

The upper 13.5 m of the core was scanned with an Avaatech XRF core scanner at NIOZ at 1-cm resolution. Detailed bulk-chemical composition records acquired by XRF core scanning allow accurate determination of stratigraphical changes as well as assessment of the contribution of the various components in lithogenic and marine sediments. The XRF core scanner uses energy dispersive fluorescence radiation to measure the chemical composition of the sediment as element intensities in total counts or counts per

second (e.g., Tjallingii et al., 2010). The measured element intensities depend on the element concentration in the sediment but also on matrix effects, physical properties, the sample geometry, and hardware settings of the scanner (Röhl and Abrams, 2000; Tjallingii et al., 2007, 2010). After cleaning and preparation of the archive-half core surface and covering with SPEXCerti Ultralene® foil, the core was measured at both 10 kV and 30 kV covering the following elements Al, Si, P, S, Cl, K, Ca, Sc, Ti, V, Cr, Mn, Fe, Co, Ni, Cu, Zn, Ga, Ge, As, Se, Br, Rb, Sr, Y, Zr, Nb, Mo, Tc, Ru, Rh, Pd, Ag, Cd, In, Sn, Sb, Te, I, Cs, Ba, Hf, Ta, W, Re, Os, Ir, Pt, Au, Hg, Tl, Pb. Log-ratios of two elements measured by XRF core scanning can be interpreted as the relative concentrations of two elements and minimizes the effects of down-core changes in sample geometry and physical properties (Weltje and Tjallingii, 2008). It is now well established that the elements Ca, Fe, and Ti can be measured reliably with the XRF-scanning method. The Log (Fe/Ca) record shown in Fig. 2 shows a clear pattern of glacial-interglacial changes. The records of Log (Ti/Ca), (Si/Al) and (Zr/Fe) shown in Fig. 3 in essence show the same (although opposite) pattern. However, in the case of the element Fe, there is a risk of measuring secondary Fe-forming minerals (cf. pyrite). For this reason, we compare the Zr/Fe record with Al/Si (Fig. 3).

5.3. Particle-size analyses

The upper 13.5 m of the core was sampled at 5-cm intervals. However, as sedimentation rates in the glacial stages are relatively low, these were sampled at higher resolution at 2.5-cm intervals. Biogenic constituents were removed from the samples to isolate the terrigenous fraction prior to particle-size analysis. First, to

remove organic carbon (Corg), 10 ml of H₂O₂ (35%) was added to approximately 500 mg of bulk sediment and the mixture was boiled until the reaction ceased and excess H₂O₂ changed into H₂O and O₂. Next, to remove calcium carbonate 10 ml of HCl (10%) in 100 ml demineralised water was added to the sediment and boiled for one minute to speed up the reaction. Visual checks were made to ensure the removal of CaCO₃ was complete. The sediment was then diluted with demineralised water until approximately neutral pH was reached. The visual checks showed that the inner fillings of a fair number of foraminifer tests with an organic-walled coating remained, which could only be removed by repeating the H₂O₂ pre-treatment step. As a last pre-treatment step, biogenic silica was removed by adding 6 g of NaOH pellets dissolved in 100 ml demineralised water to the sediment and the mixture was boiled for 10 min. Visual checks were made periodically to ensure the removal of all diatoms and radiolarians. The solution was diluted with demineralised water to a neutral pH. Immediately prior to particle size analysis, 10 ml of dissolved sodium pyrophosphate (Na₄P₂O₇*10H₂O) was added to the now Corg-, CaCO₃-, and biogenic opal-free sediment (i.e. terrigenous fraction) to ensure disaggregation of potential aggregates.

Particle size distributions of the terrigenous fraction were measured with a Coulter laser particle sizer LS230 at NIOZ, which resulted in 116 size classes from 0.4 to 2000 µm for every analysed sample.

5.4. End-member modelling

The end-member modelling technique of Weltje (1997) was consequently applied to the measured particle-size distributions, to

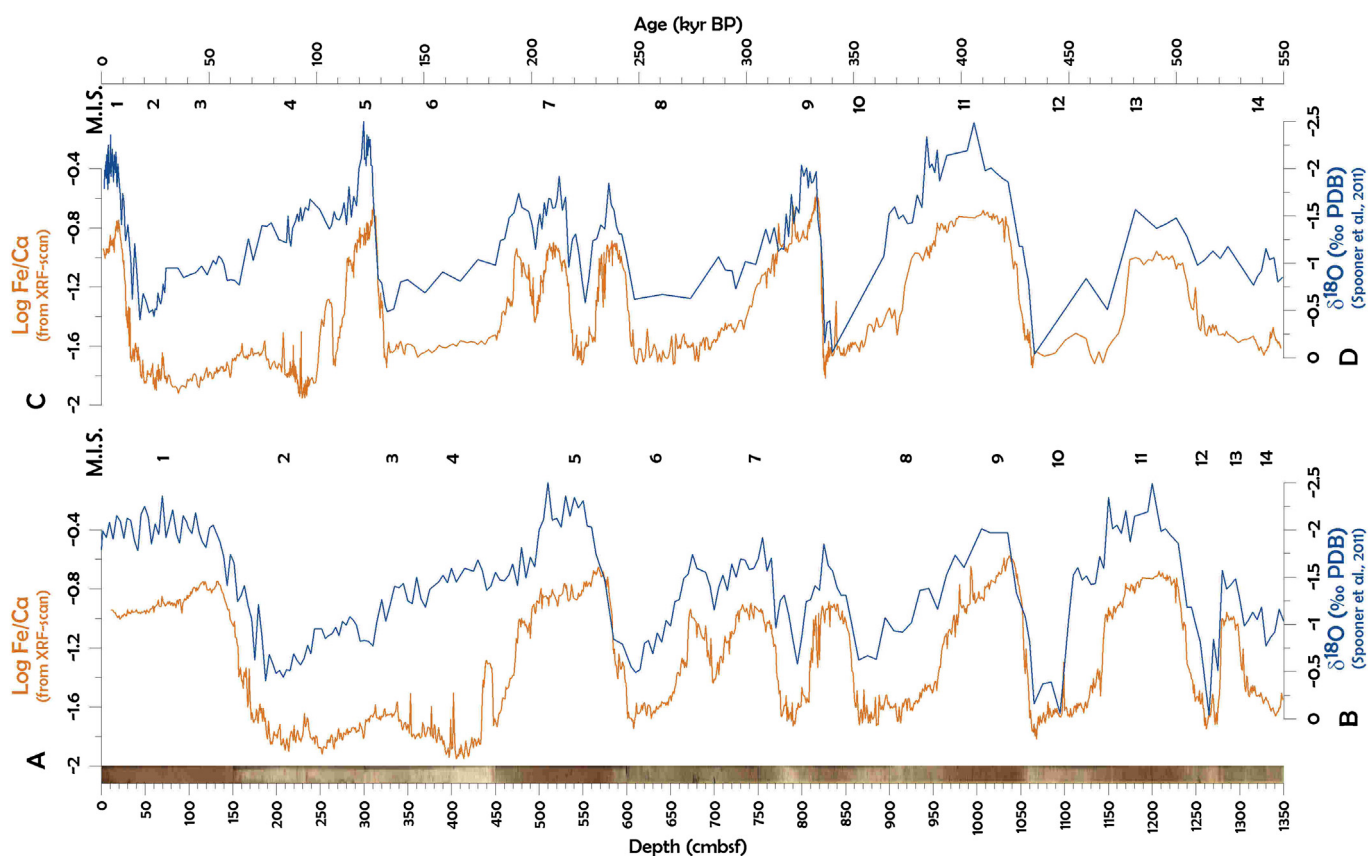


Fig. 2. Stratigraphy of the upper 13.50 m of core MD00-2361 shown by an alternation of dark brown and pale layers in the bottom photograph. A) Log (Fe/Ca) from XRF scan, plotted with B) $\delta^{18}\text{O}$ (‰ PDB) from Spooner et al., 2011, on a depth scale; C) Log (Fe/Ca) from XRF scan, plotted with D) $\delta^{18}\text{O}$ (‰ PDB) from Spooner et al., 2011 on an age scale, based on the age model of Spooner et al. (2011). Marine Isotope Stages (M.I.S.) are indicated.

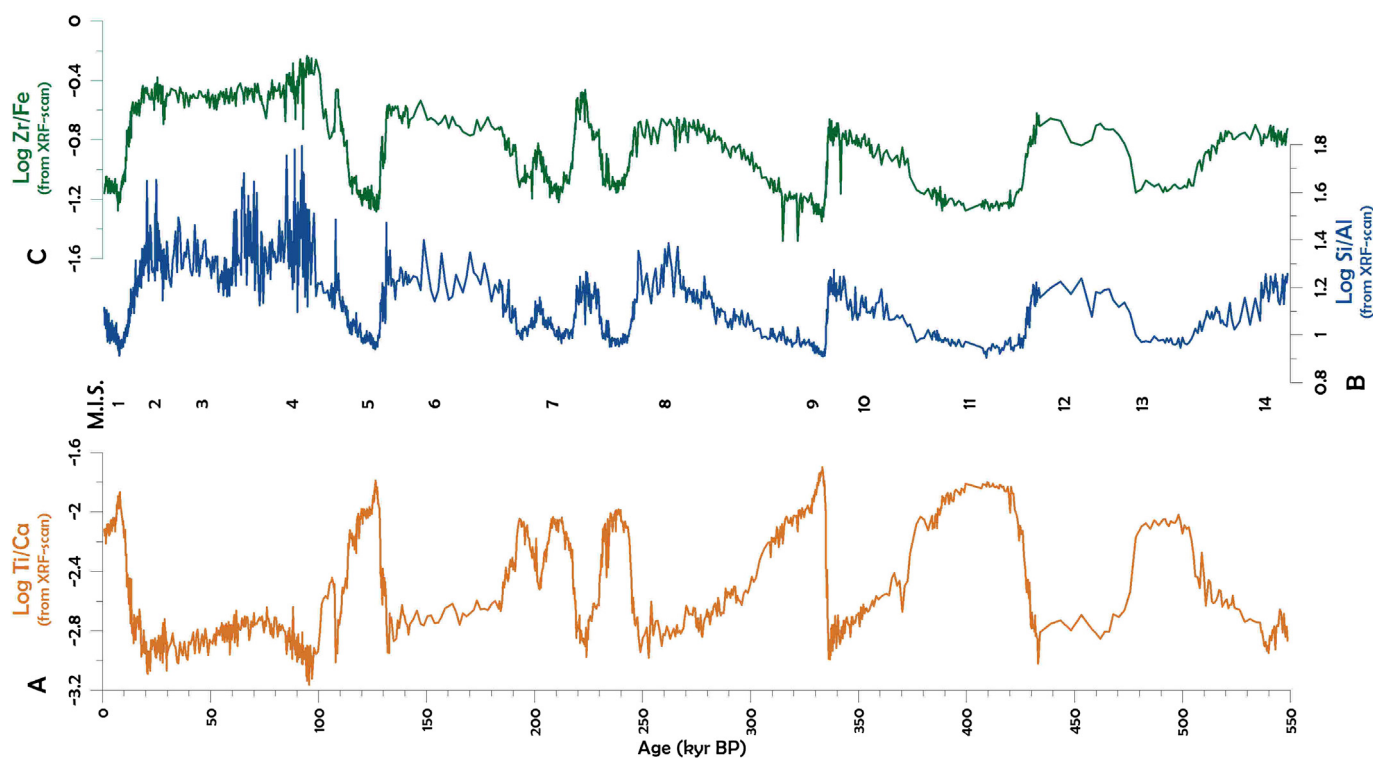


Fig. 3. Bulk-chemical records from XRF scans A) Log (Ti/Ca), B) Log (Si/Al), and C) Log (Zr/Fe). Marine Isotope Stages (M.I.S.) are indicated in the middle.

determine the proportions of distinct sediment components contributing to the overall, measured particle-size signal. To estimate the minimum number of end members required for a satisfactory approximation of the data, the coefficients of determination were calculated. The latter represents the proportion of the variance of each grain-size class that can be reproduced by the approximated data. This proportion is equal to the squared correlation coefficient (r^2) of the input variables and their approximated values (Weltje, 1997; Prins and Weltje, 1999). Based on the parsimony between number of end members and goodness-of-fit, combined with the eventual particle-size distributions of the end members, the number of end members was chosen. In previous studies where the end-member approach was applied to deep-marine sediments (Prins and Weltje, 1999; Stuut et al., 2002; Weltje and Prins, 2003; Stuut et al., 2007; Tjallingii et al., 2008; Filipsson et al., 2011) as well as loess deposits (Prins and Vriend, 2007; Prins et al., 2007), the modelled sub-populations were all uniform, unimodal grain-size distributions, although no shape is pre-scribed in the model. This is obvious as there is no natural sorting process that would result in polymodal sediment deposits. There is one exception to this observation: ice-rafted sediments, which are not sorted at all, and which is also recognised by the end-member model (e.g., Prins et al., 2002).

6. Results and interpretation

6.1. Stratigraphy

Core MD00-2361 consists of alternating brown clay-rich bands and light-grey foram-rich intervals (Fig. 2). These distinct colour differences are also reflected in the XRF records: the log ratio of Fe/Ca shows high values during clay-rich interglacial stages and low values during CaCO_3 -rich glacial stages (Fig. 2). For this reason, the Fe/Ca log-ratio and $\delta^{18}\text{O}$ ratio (Spooner et al., 2011) vary in parallel. The age model of Spooner et al. (2011), which is based on oxygen-

isotope stratigraphy and 12 AMS ^{14}C dates, was adopted for this study. From the age-depth conversion (Fig. 2), it becomes clear that compaction of the sediments increases towards the lower part of the studied interval (viz. the upper 13.6 m of the core).

6.2. X-ray fluorescence

Many studies have tried to derive proxies from XRF scans of marine sediment cores and thus far it has been determined that the relative variation of terrigenous and marine constituents can be best deduced from the elements Titanium (Ti) and Calcium (Ca). The conservative element Ti is restricted to lithogenic sediments and inert to diagenetic process (Calvert and Pedersen, 2007; Tjallingii et al., 2010; Bloemsmma et al., 2012). The element Ca is a measure for the abundance of biogenic carbonates (CaCO_3) in marine sediments (Arz et al., 1998; Tjallingii et al., 2010). The Ti/Ca ratio in core MD00-2361 shows high values during interglacial stages, which are dominated by brown mud that we interpret as being derived from fluvial runoff. During glacial stages, on the other hand, the input of these rivers seems to drop, terrigenous sediment input rates drop and the marine sediments are dominated by CaCO_3 from biogenic constituents such that of foraminifera, coccoliths and pteropods. This results in low Ti/Ca values (Fig. 3A).

Next to the general distinction between land-derived and marine sediments, following (Mulitza et al., 2008) we use the down-core XRF-scans to distinguish between aeolian dust and fluvial muds by examining the log-ratio of Silicon (Si) over Aluminium (Al, Fig. 3B), and the log-ratio of Zircon (Zr) over Iron (Fe, Fig. 3C). As the biogenic silica fraction (diatom remains) is very low (<2% as estimated from microscope analyses), the element Si is predominantly present as quartz grains, whereas Al clearly indicates aluminosilicates which are mostly present in fluvial sediments (e.g., Reichart et al., 1997; Mulitza et al., 2008). This observation is corroborated by microscope analyses of sediment particles; relatively large sand-sized particles can be observed, which show typical aeolian

features such as pitted- and rounded surfaces on quartz grains (Fig. 4). In addition, the wind-blown fraction is enriched in Zr due to its presence in heavy minerals (e.g., Matthewson et al., 1995). Fe, on the other hand, is enriched in heavily weathered soils (Mulitza et al., 2008) and, when predominantly present as coating on particles, this element is enriched in the fine fraction.

The log-ratios of both Si/Al and Zr/Fe show a very similar pattern (Fig. 3), but which is opposite to that of Ti/Ca. Low values of Si/Al and Zr/Fe occur during interglacial stages and high values during glacial stages, which we interpret as increased aeolian input during glacial stages as opposed to dominant fluvial input during interglacial stages.

6.3. Particle size of the terrigenous fraction

The results of the particle-size analyses ($n = 438$), after dissolution of the biogenic fraction, are shown in Fig. 5 where the raw particle-size data are presented as a contour plot of the 116 size classes against age in the core (Fig. 5D). The particle-size record and the *G. ruber* $\delta^{18}\text{O}$ record show very similar patterns over time, indicating relatively fine-grained sediment deposition during interglacial stages (MIS 1, 3, 5, 7, 9, and 11) and relatively coarse-grained sediment deposition during glacial stages (MIS 2, 4, 6, 8, 10, and 12). This reflects a different wind regime with generally increased wind strengths during glacial periods.

In addition, the median particle size is plotted versus age in Fig. 5C. The median particle sizes vary between 2.8 and 122 μm , and this clearly reflects the trends in the raw data shown in Fig. 5D with lower median sizes during interglacial stages compared to glacial stages. Based on the age model by Spooner et al. (2011), which was constructed using the oxygen isotopes of the near-surface dweller *G. ruber* (Fig. 2A), linear sedimentation rates were calculated (Fig. 5B), which vary between 0.3 and 28 cm/ka. The sedimentation rates show a distinct pattern of markedly lower values during glacial stages compared to interglacial stages.

6.4. End-member modelling

The particle-size distributions of the terrigenous sediment fraction in core MD00-2361 show multi-modal distributions with peaks around 10 and 80 μm (Fig. 6A). For these size distributions, end-member models were calculated with increasing number of end members. Fig. 6B shows the coefficients of determination (r^2) plotted against particle size for models with 2–10 end members. The mean coefficient of determination of the particle-size classes increases when the number of end members increases (Fig. 6C). The end-member models with 2–5 end members all show relatively low r^2 for the size range $<2 \mu\text{m}$ (Fig. 6B). This explains why the values for the mean r^2 for these models (Fig. 6C) are relatively low, between 0.42 and 0.73. Based on the goodness-of-fit statistics and the shape of the end-member size distributions, we chose the three end-member model as the best balance between minimum number of end members and maximum goodness-of-fit.

The particle-size distributions of the three end members are shown in Fig. 6D. All end members have a clearly defined dominant mode. End member EM1 has a modal grain size of $\sim 80 \mu\text{m}$, end member EM2 of $\sim 15 \mu\text{m}$, and end member EM3 has a modal grain size of $\sim 5 \mu\text{m}$. As for similar studies carried out on cores to distinguish aeolian sediments deposited offshore large deserts [Namib Desert: Stuut et al. (2002); Atacama Desert: Stuut et al. (2004); Sahara Desert: Stuut et al. (2005); Hamann et al. (2008); McGregor et al. (2009); Filipsson et al. (2011)], we interpret these end members as representing the wind-blown fraction (EM1 and EM2), and a fluvially-derived one (EM3). The change in the size of the aeolian fraction in essence has the potential to be used as a proxy for wind strength (e.g., Stuut et al., 2002). However, this is not always the case in all settings, for reasons that we do not yet comprehend. In sediment records off NW Africa, the ratio of the two aeolian end members did not seem to make any sense, and also for this particular sediment core off NW Australia, the ratio of the two aeolian end members does not show a pattern in any way similar to

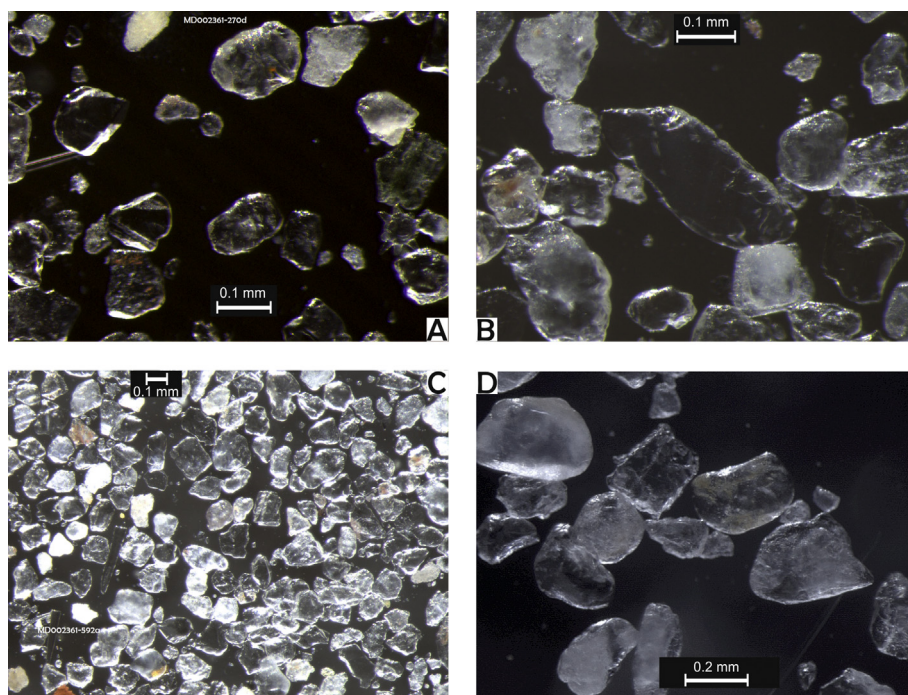


Fig. 4. Light-microscope images of some selected samples from core MD00-2361 after removal of all the marine organic material (see Methods section). Note the roundness of the large quartz particles. **A)** $>90 \mu\text{m}$ sieve fraction at 250 cm depth (MIS2), **B)** and **C)**, $>90 \mu\text{m}$ sieve fraction at 592 cm depth (MIS6), **D)** bulk fraction at 1070 cm depth (MIS10). Note that the scale bars in Figs. **A**, **B**, and **C** are 100 μm , and in **D** 200 μm .

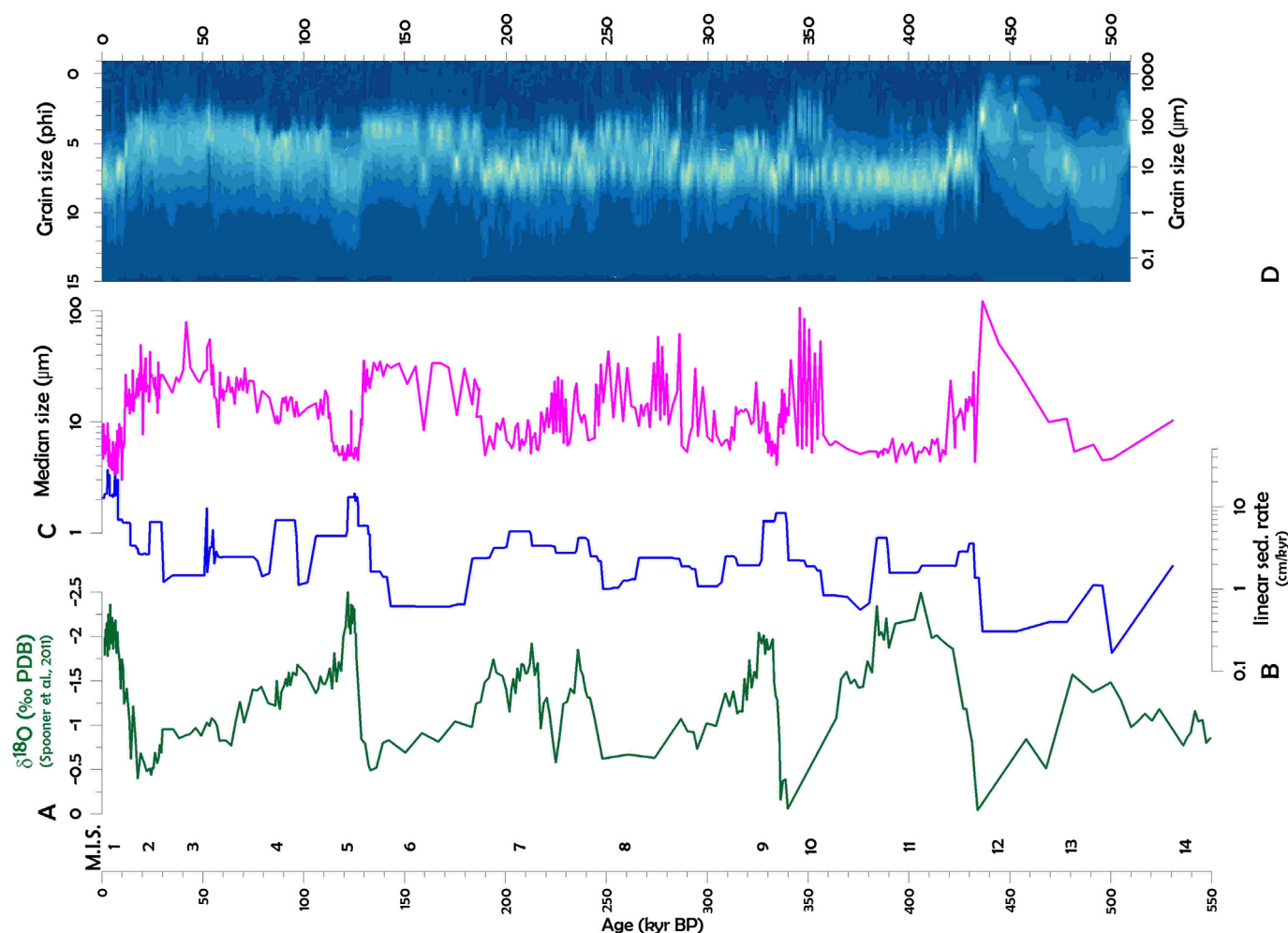


Fig. 5. Downcore records of core MD00-2361 for the last 550,000 years. A) $\delta^{18}\text{O}$ (‰ PDB, from Spooner et al. (2011)); B) sedimentation rates, calculated using the age model by Spooner et al., 2011; C) Median grain size of the terrigenous sediment fraction. Grey bars indicate glacial marine isotope stages; D) contour plot of the grain-size distributions of the terrigenous sediment fraction. Top x-axis in phi [$-2\log(d)$], bottom x-axis in micrometres on log scale. Marine Isotope Stages (M.I.S.) are indicated at the bottom.

the other proxy records. We assume that this has to do with the end-member modelling algorithm, which sometimes has problems to tease apart the coarse-sediment fraction. If the proportion of one of the aeolian end members is very low or zero, the ratio gets very noisy. For this reason, we decided not to zoom into the aeolian fraction, but instead to present it as the total-dust fraction in Fig. 7.

The down-core record of the relative contributions of the end members is shown in Fig. 7B and D, where the ratio of the fluvial and aeolian end members is considered as a proxy for continental aridity (e.g., Stuut et al., 2002), and the sum of the two wind-blown end members is considered a proxy for total dust (e.g., Stuut et al., 2002).

7. Mid- to Late Quaternary of Western Cape aridity signals and trade-wind intensity

Aeolian sediments deposited in the deep sea close to the continent usually are coarser grained than hemipelagic sediments; terrigenous sediments with median grain size larger than $6\ \mu\text{m}$ are generally attributed to aeolian transport, and smaller than $6\ \mu\text{m}$ to hemipelagic transport. This is based on deep-sea sediment studies (Koopmann, 1981; Sarnthein et al., 1981; Sirocko et al., 1991; Prins and Weltje, 1999; Prins et al., 2000) as well as modern-dust studies during which dust was collected at sea (e.g., Clemens, 1998; Rattmeyer et al., 1999; Stuut et al., 2005). As a consequence,

in our sediment core from the northwestern Western Australian continental slope, the end-member fraction EM1 and EM2 are considered of aeolian, and EM3 of fluvial origin. Support for this interpretation comes from light-microscope observations which show that these coarse particles are well-rounded, which is typical for an aeolian origin (Fig. 4) (e.g., Pye, 1987). Following comparable studies on aeolian sediments deposited offshore large deserts (e.g., Prins and Weltje, 1999; Stuut et al., 2002, 2004, 2005; Hamann et al., 2008; McGregor et al., 2009; Filipsson et al., 2011; Meyer et al., 2013), we use the ratio of wind-blown versus fluvial material in sediment core MD00-2361 as a proxy for continental aridity in North West Cape (Fig. 7B). The 550-ka record offshore northwestern Western Australian shows pronounced and persistent arid conditions during glacial stages and clearly more humid conditions during interglacial stages. The variability in the aridity record is very comparable to the Log (Ti/Ca) record (Fig. 7A), which we believe can be used to indicate the total flux of land-derived sediments. Considering the variability in the sedimentation rates, which also shows roughly the same glacial–interglacial pattern, we hypothesise that indeed the last seven interglacial stages (down to MIS 13) were characterised by increased (seasonal) rainfall, which led to increased fluvial runoff and a large supply of hemipelagic clays to the continental slope. During glacial stages, decreased rainfall would have led to a dominance of wind-blown sediments at much lower input rates, leading to a larger dilution of the total sediment by

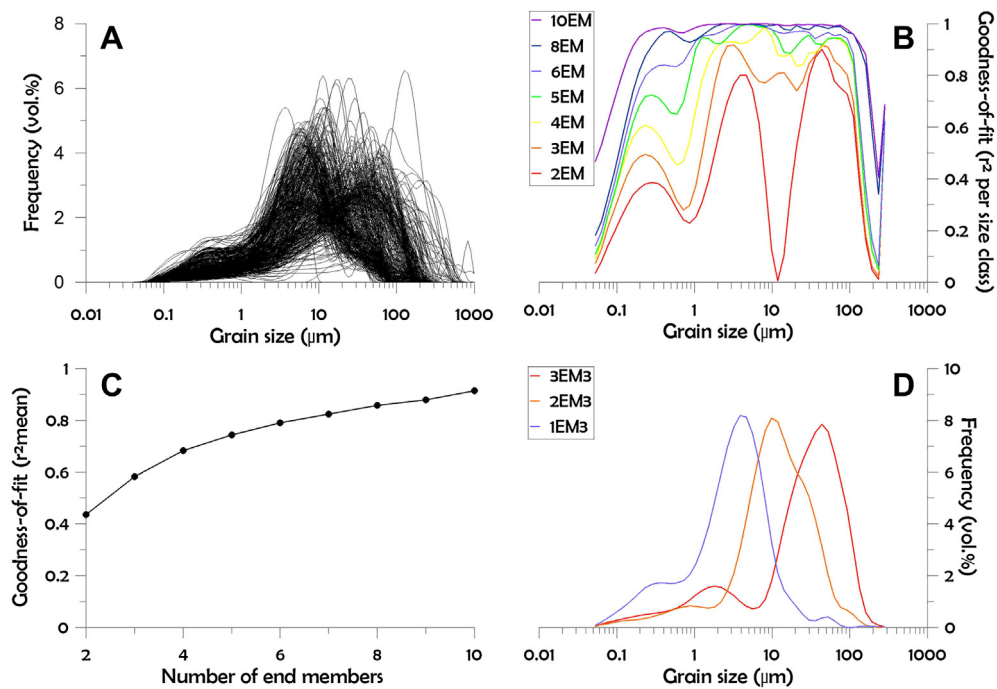


Fig. 6. End-member modelling results. **A**) Raw grain-size distributions of the entire data set ($N = 438$); **B**) Goodness-of-fit statistics per size class for seven end-member models with 2–10 end members; **C**) Mean goodness-of-fit, averaged per end-member model for models with 2–10 end members; **D**) The grain-size distributions of the end members in the three end-member model. See text for more details.

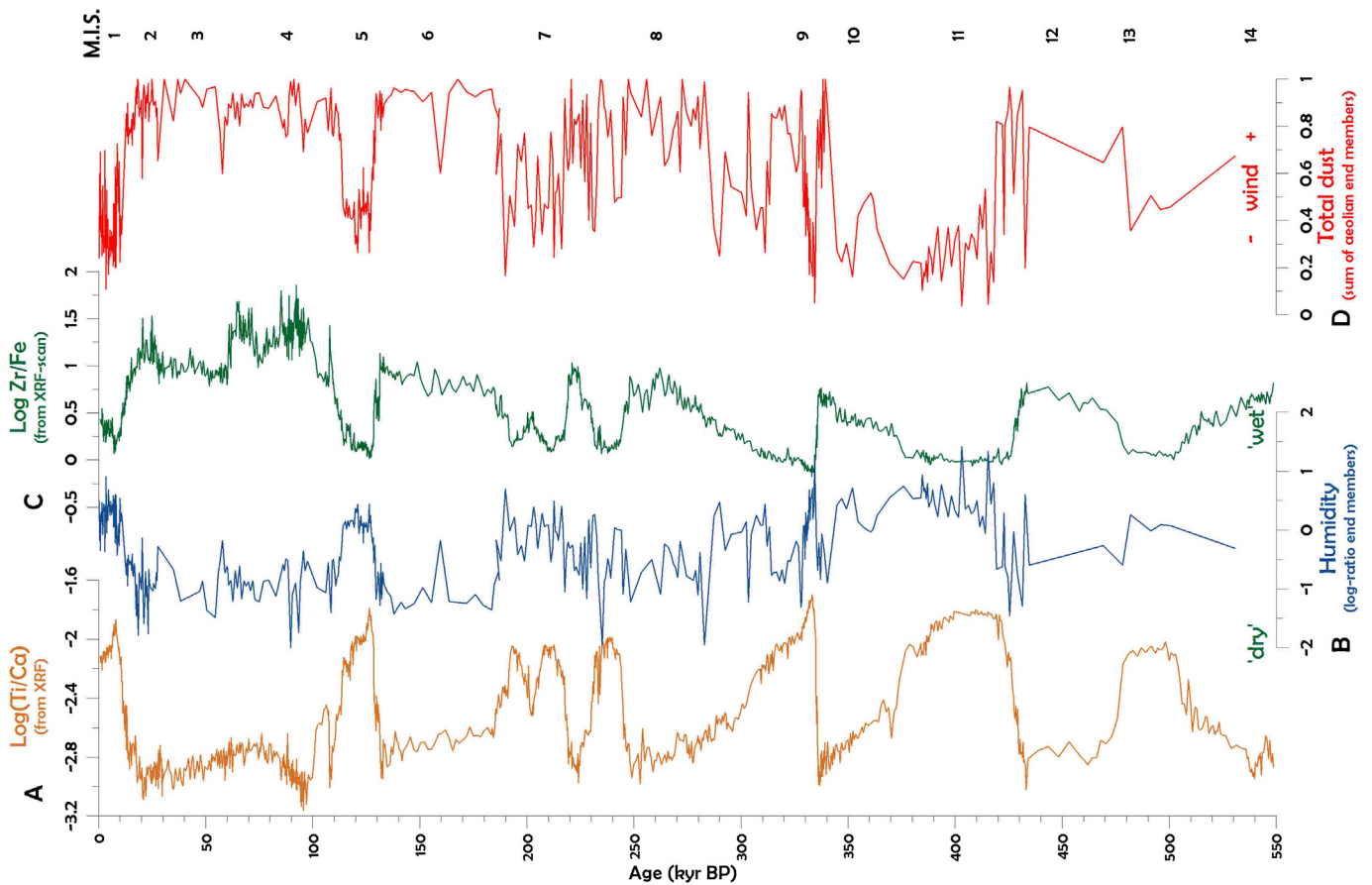


Fig. 7. Downcore records of MD00-2361 which are interpreted in terms of palaeoenvironmental conditions in North West Cape. **A**) Log Ti/Ca, a proxy for land-derived sedimentation; **B**) Continental humidity, expressed as a log-ratio of the fluvial and aeolian end members; **C**) Log (Zr/Fe), a proxy for continental humidity; **D**) Total dust, expressed as the sum of the two aeolian end members. Marine Isotope Stages (M.I.S.) are indicated at the top.

marine carbonates. However, the overall size of these aeolian particles strongly increased during glacial stages compared to interglacial stages, which can only be explained by an increase in atmospheric circulation; increased trade-wind intensities during these glacial stages. This finding is supported by the synchronous variations of both the Log (Zr/Fe) and total dust records (Fig. 7C and D) which show increased values during glacial stages and lower values during interglacial stages. In addition, the Log (Zr/Fe) shows an increasing amplitude of changes towards the younger portion of the core (Fig. 7C). Although the grain-size derived proxy record does not show a similar increase in total dust from 550 ka BP towards present, we believe the increase in Zr/Fe is real and not related to a decrease in compaction towards the top of the core as we do not observe the same trend in the other bulk-chemical records.

The pacing of the palaeoenvironmental changes in North West Cape follows the typical northern hemisphere pattern, which is opposite to palaeo-environmental reconstructions established for Chile (Lamy et al., 2004; Stuut and Lamy, 2004) and South Africa (Stuut et al., 2002, 2004; Chase and Meadows, 2007) at approximately the same latitude $\sim 20^\circ\text{S}$. The climate in these other regions on the southern hemisphere is dictated by latitudinal movements of the rain-bearing southern westerlies. We argue that contrary to both South America and South Africa, Australia is a large landmass, covering more than almost 40° of longitude, which is so large that it can still develop its own monsoonal system that is strong enough not to be affected by the northward displacement of the frontal zones from the Southern Ocean. We compared our record with the record presented by Tachikawa et al. (2011) and concluded that there is no similarity whatsoever between the records, probably thanks to the fact that their signal is a combination of runoff from Indonesian rivers and ocean productivity, whereas our record registers Australian continental climate.

Bowler (1975) already had suggested that the summer anticyclone in full glacial time was positioned some 5° further north than today. We refer to the general maps of wind directions for today and during the LGM already provided in Gingele et al. (2001). Together with intensified pressure gradients, such a shift would assist in the strengthening westerly flow as required by the origin and orientation of dunes built at this time. Such a shift, consistent with the great expansion of Antarctic summer sea ice (Hays et al., 1976) and coinciding with exposure of large areas of the continental shelf, would greatly accentuate the influence of warm continental air masses on the more humid semi-arid margins. Consequently, outbreaks of dry air from the continental interior were probably more frequent in full glacial summers than they are today. However, in northern Australia the southeasterly trades, though greatly intensified, would have maintained directions similar to those of today. We hypothesise that there may be locations on the southwest Australian continental slope that record the history of northward shifting southern westerlies, just offshore the winter-rain region of South Australia.

As observed today the dune fields south and east of the Exmouth peninsula are vegetated and dunes are inactive, thus supplying little aeolian sediment to sea. Nevertheless, deflation still does occur today during very dry years or after extensive fires, when vegetation consisting of grasses and shrubs are completely destroyed and dunes surfaces exposed to wind erosion. We anticipate that during glacial periods, a hydrological deficit paralleled by colder temperatures (e.g., van der Kaars and De Deckker, 2002; Spooner et al., 2011) would have decreased the vegetation cover that would have helped towards dune mobility.

We compared the XRF data along the section of the core studied here and, in particular, between interglacials MIS11 and MIS5e – as MIS11 is considered to have been as warm if not even warmer than the MIS5e as well as the Holocene – and glacials MIS12 and 2 –

MIS12 having been considered to be the coldest glacial during the Brunhes Chron (Raymo and Mitrovica, 2012). We note that despite the fact that MIS11 extends for a much longer period, viz. 50,000 years, river discharge (as seen through Fe/Ca) did for about the same period, but values were similar to those for MIS5e and the Holocene, thus pointing to similar river discharges even if it was for a more extensive period. MIS13, on the other hand, registered much lower Fe/Ca values (Fig. 3). Spooner et al. (2011)'s mean SST values never reached the highest ones in MIS5e.

For MIS12, on the other hand, the Zr/Fe values never reached those seen in the Last Glacial (Fig. 3), therefore suggesting that conditions were not as arid as considered in other parts of the globe (Pierre et al., 2001). This is further corroborated when examining the Si/Al values (Fig. 3), which also show that the amplitude of the record increases from the eldest part of the record to the present. The largest amplitudes are interpreted as broad glacial–interglacial environmental variability, especially during the Last Glacial–Interglacial cycle.

8. Conclusions

The terrigenous fraction of sediments from a deep-sea sediment core recovered in the SE Indian Ocean from the northwestern continental slope of Western Australia, reveals a history of Western Australian climate throughout the last 550 ka. End-member modelling of a data set of grain-size distributions ($n = 438$) of the terrigenous sediment fraction, combined with bulk-chemical analyses using an XRF scanner allows to interpret the record in terms of fluvial and aeolian sediment deposition, both related to palaeo-environmental conditions in the north-western portion of Western Australia. The mid- to late Quaternary climate in Western Australia was relatively arid during the glacial stages and relatively humid during the interglacial stages, owing to meridional shifts in the atmospheric circulation system. Opposite to published palaeo-environmental records from the same latitude (20°S) offshore Chile and offshore Namibia, the Australian aridity record does not show the typical southern hemisphere climate variability of humid glacials and dry interglacials, which we interpret to be the result of the relatively large landmass of the Australian continent, which causes a strong monsoonal climate pattern.

Our investigations dome on core MD00-2361 which span the last 550 ka of sedimentation clearly identifies wet and dry periods that coincide with interglacial and glacial periods, respectively but none of them were of the same amplitude. Already our work has some implications for the long-term history of aridity in Australia that has obvious implications for the evolution of the Australia biota adapted to aridity. Additional investigations on the other sections of core MD00-2361, which we believe span the last 1.5 Ma of sedimentation, will give light on the subject.

Acknowledgements

We thank the captain and crew (namely Y. Balut) and scientists (namely F. Guichard) aboard R.V. *Marion Dufresne* for their help with coring and sampling operations during the TIP 2000 expedition. We thank Gert-Jan Weltje for making the end-member modelling algorithm (EMMA) available. We greatly acknowledge Rineke Gieles for her substantial support with the XRF scanning of the core. This work was financed by NIOZ and ARC discovery grant DP0772180, and an ERASMUS grant that allowed Felix Temmesfeld a research stay at NIOZ to carry out most of the grain size analyses. We acknowledge the financial support within the SCAN-2 project for advanced instrumentation by the Netherlands Science Foundation (NWO).

References

- Arz, H.W., Pätzold, J., Wefer, G., 1998. Correlated millennial-scale changes in surface hydrography and terrigenous sediment yield inferred from Last-Glacial marine deposits off NE Brazil. *Quat. Res.* 50, 157–166.
- Bloemsmas, M.R., Zabel, M., Stuut, J.B.W., Tjallingii, R., Collins, J.A., Weltje, G.J., 2012. Modelling the joint variability of grain size and chemical composition in sediments. *Sediment. Geol.* 280, 135–148.
- Bowler, J.M., 1975. Glacial age aeolian events at high and low altitudes: a southern hemisphere perspective. In: Van Zinderen Bakker, E.M. (Ed.), *Antarctic Glacial History and World Palaeoenvironments*. Balkema, Rotterdam, pp. 149–172.
- Bowler, J.M., 1976. Aridity in Australia: age, origins and expression in aeolian landforms and sediments. *Earth-Sci. Rev.* 12, 279–310.
- Calvert, S.E., Pedersen, T.F., 2007. Chapter fourteen elemental proxies for palaeoclimatic and palaeoceanographic variability in marine sediments: interpretation and application. In: Claude, H.M., Anne De, V. (Eds.), *Developments in Marine Geology*. Elsevier, pp. 567–644.
- Chase, B.M., Meadows, M.E., 2007. Late Quaternary dynamics of southern Africa's winter rainfall zone. *Earth-Sci. Rev.* 84, 103–138.
- Clemens, S.C., 1998. Dust response to seasonal atmospheric forcing: proxy evaluation and calibration. *Paleoceanography* 13, 471–490.
- De Deckker, P., Corrége, T., Head, J., 1991. Late Pleistocene record of cyclic eolian activity from tropical Australia suggesting the Younger Dryas is not an unusual climatic event. *Geology* 19, 602–605.
- De Deckker, P., Tapper, N.J., van der Kaars, S., 2002. The status of the Indo-Pacific Warm Pool and adjacent land at the Last Glacial Maximum. *Glob. Planet. Change* 35, 25–35.
- De Deckker, P., Moros, M., Perner, K., Jansen, E., 2012. Influence of the tropics and southern westerlies on glacial interhemispheric asymmetry. *Nat. Geosci.* 5, 266–269.
- Dodson, W.J., 2009. Groundwater Recharge from the Gascoyne River, Western Australia. Hydrogeological Record Series Report No. HG 32. Department of Water, Western Australian Government, Perth. Available at: <http://www.water.wa.gov.au/PublicationStore/first/79231.pdf>.
- Ehlert, C., Frank, M., Haley, B.A., Böniger, U., De Deckker, P., Gingele, F.X., 2011. Current transport versus continental inputs in the eastern Indian Ocean: radiogenic isotope signatures of clay size sediments. *Geochem. Geophys. Geosystems* 12, Q06017.
- Filipsson, H.L., Romero, O.E., Stuut, J.-B.W., Donner, B., 2011. Relationships between primary productivity and bottom-water oxygenation off northwest Africa during the last deglaciation. *J. Quat. Sci.* 26, 448–456.
- Gingele, F.X., De Deckker, P., Hillenbrand, C.-D., 2001. Late Quaternary fluctuations of the Leeuwin Current and palaeoclimates on the adjacent land masses: clay mineral evidence. *Aust. J. Earth Sci. Int. Geosci. J. Geol. Soc. Aust.* 48, 867–874.
- Hamann, Y., Ehrmann, W., Schmiedl, G., Kruger, S., Stuut, J.-B.W., Kuhnt, T., 2008. Sedimentation processes in the Eastern Mediterranean Sea during the Late Glacial and Holocene revealed by end-member modelling of the terrigenous fraction in marine sediments. *Mar. Geol.* 248, 97–114.
- Hays, J.D., Lozano, J.A., Shackleton, N.J., Irving, G., 1976. Reconstruction of the Atlantic and western Indian Ocean sectors of the 18,000 BP Antarctic Ocean. In: Cline, R.M., Hays, J.D. (Eds.), *Investigation of Late Quaternary Paleoclimatology and Paleoclimatology*. Geological Society of America, Boulder, pp. 337–372.
- Hesse, P.P., 1994. The record of continental dust from Australia in Tasman sea sediments. *Quat. Sci. Rev.* 13, 257–272.
- Hesse, P.P., McTainsh, G.H., 2003. Australian dust deposits: modern processes and the Quaternary record. *Quat. Sci. Rev.* 22, 2007–2035.
- Hesse, P.P., Magee, J.W., van der Kaars, S., 2004. Late Quaternary climates of the Australian arid zone: a review. *Quat. Int.* 118–119, 87–102.
- Holz, C., Stuut, J.-B.W., Henrich, R., 2004. Terrigenous sedimentation processes along the continental margin off NW-Africa: implications from grain-size analyses of surface sediments. *Sedimentology* 51, 1145–1154.
- Humphreys, W.F. (Ed.), 1993. *The Biogeography of Cape Range, Western Australia: Being the Proceedings of a Symposium Held under the Auspices of the Western Australian Museum in Perth on 21 November 1992 at the Art Gallery of Western Australia*. Western Australian Museum, Perth.
- Koopmann, B., 1981. Sedimentation von Saharastaub im subtropischen Nordatlantik während der letzten 25.000 Jahre. *Meteor. Forschungsergebnisse C* 35, 23–59.
- Lamy, F., Kaiser, J., Ninnemann, U., Hebbeln, D., Arz, H.W., Stoner, J., 2004. Antarctic timing of surface water changes off Chile and Patagonian Ice Sheet response. *Science* 304, 1959–1962.
- Leighton, K., Mitchell, A., 1997. Report on Damage Caused by the Flood on the Ashburton River in February 1997. Department of Land Administration, Perth, Western Australia.
- Matthewson, A.P., Shimmield, G.B., Kroon, D., 1995. A 300 kyr high-resolution aridity record of the North-African continent. *Paleoceanography* 10, 677–692.
- McGee, D., deMenocal, P.B., Winckler, G., Stuut, J.B.W., Bradtmiller, L.L., 2013. The magnitude, timing and abruptness of changes in North African dust deposition over the last 20,000 years. *Earth Planet. Sci. Lett.* 371–372, 163–176.
- McGregor, H.V., Dupont, L., Stuut, J.-B.W., Kuhlmann, H., 2009. Vegetation change, goats, and religion: a 2000-year history of land use in southern Morocco. *Quat. Sci. Rev.* 28, 1434–1448.
- McTainsh, G., 1989. Quaternary aeolian dust processes and sediments in the Australian region. *Quat. Sci. Rev.* 8, 235–253.
- Meyer, I., Davies, G.R., Vogt, C., Kuhlmann, H., Stuut, J.-B.W., 2013. Changing rainfall patterns in NW Africa since the Younger Dryas. *Aeolian Res.* 10, 111–123. <http://dx.doi.org/10.1016/j.aeolia.2013.03.003>.
- Montero-Serrano, J.C., Bout-Roumazeilles, V., Sionneau, T., Tribouillard, N., Bory, A., Flower, B.P., Riboulleau, A., Martinez, P., Billy, I., 2010. Changes in precipitation regimes over North America during the Holocene as recorded by mineralogy and geochemistry of Gulf of Mexico sediments. *Glob. Planet. Change* 74, 132–143.
- Mulitza, S., Prange, M., Stuut, J.-B.W., Zabel, M., von Dobeneck, T., Itambi, A.C., Nizou, J., Schulz, M., Wefer, G., 2008. Sahel megadroughts triggered by glacial slowdowns of Atlantic meridional overturning. *Paleoceanography* 23. <http://dx.doi.org/10.1029/2008PA001637>.
- New, M., Lister, D., Hulme, M., Makin, I., 2002. A high-resolution data set of surface climate over global land areas. *Clim. Res.* 21, 1–25.
- Olley, J.M., De Deckker, P., Roberts, R.G., Fifield, L.K., Yoshida, H., Hancock, G., 2004. Optical dating of deep-sea sediments using single grains of quartz: a comparison with radiocarbon. *Sediment. Geol.* 169, 175–189.
- Pierre, C., Saliege, J.F., Urrutiaguer, M.J., Giraudeau, J., 2001. Stable isotope record of the last 500 k.y. at Site 1087 (Southern Cape Basin). In: Wefer, G., Berger, W.H., Richter, C. (Eds.), *Proceedings of the ODP Scientific Results, Ocean Drilling Program, College Station, TX*, pp. 1–22.
- Prins, M.A., Stuut, J.-B.W., Lamy, F., Weltje, G.J., 1999. End-member modelling of grain-size distributions of deep-sea detrital sediments and its palaeoclimatic significance: examples from the NW Indian, E Atlantic and SE Pacific Oceans. *Geophys. Res. Abstr.* 1, 564.
- Prins, M.A., Weltje, G.J., 1999. End-member modeling of siliciclastic grain-size distributions: the Late Quaternary record of eolian and fluvial sediment supply to the Arabian Sea and its paleoclimatic significance. In: Harbaugh, J., Watney, L., Rankey, G., Slingerland, R., Goldstein, R., Franseen, E. (Eds.), *Numerical Experiments in Stratigraphy: Recent Advances in Stratigraphic and Sedimentologic Computer Simulations, SEPM Special Publication 62*. Society for Sedimentary Geology, pp. 91–111.
- Prins, M.A., Postma, G., Cleveringa, J., Cramp, A., Kenyon, N.H., 2000. Controls on terrigenous sediment supply to the Arabian Sea during the late Quaternary: the Indus Fan. *Mar. Geol.* 169, 327–349.
- Prins, M.A., Bouwer, L.M., Beets, C.J., Troelstra, S.R., Weltje, G.J., Kruk, R.W., Kuijpers, A., Vroon, P.Z., 2002. Ocean circulation and iceberg discharge in the glacial North Atlantic: inferences from unmixing of sediment size distribution. *Geology* 30, 555–558.
- Prins, M.A., Vriend, M., 2007. Glacial and interglacial eolian dust dispersal patterns across the Chinese Loess Plateau inferred from decomposed loess grain-size records. *Geochem. Geophys. Geosystems* 8.
- Prins, M.A., Vriend, M., Nugteren, G., Vandenbergh, J., Lu, H., Zheng, H., Jan Weltje, G., 2007. Late Quaternary aeolian dust input variability on the Chinese Loess Plateau: inferences from unmixing of loess grain-size records. *Quat. Sci. Rev.* 26, 230–242.
- Pye, K., 1987. *Aeolian Dust and Dust Deposits*. Academic Press, London.
- Ratmeyer, V., Fischer, G., Wefer, G., 1999. Lithogenic particle fluxes and grain size distributions in the deep ocean off northwest Africa: implications for seasonal changes of aeolian dust input and downward transport. *Deep Sea Res. I Oceanogr.* 46, 1289–1337.
- Raymo, M.E., Mitrovica, J.X., 2012. Collapse of polar ice sheets during the stage 11 interglacial. *Nature* 483, 453–456.
- Rea, D.K., Janecek, T.R., 1981. Mass-accumulation rates of the non-authigenic crystalline (eolian) component of deep-sea sediments from the western Mid-Pacific Mountains. In: Stout, L.N. (Ed.), *Initial Reports of the Deep Sea Drilling Project Site 463*. NSF, Washington, pp. 653–659.
- Rea, D.K., 1994. The paleoclimatic record provided by eolian deposition in the deep sea: the geologic history of wind. *Rev. Geophys.* 32, 159–195.
- Reichert, G.J., Den Dulk, M., Visser, H.J., Van der Weijden, C.H., Zachariasse, W.J., 1997. A 225 kyr record of dust supply, paleoproductivity and the oxygen minimum zone from the Murray Ridge (northern Arabian Sea). *Palaeogeogr. Palaeoclimatol. Palaeoecol.* 134, 149–169.
- Röhl, U., Abrams, L.J., 2000. High-resolution, downhole, and nondestructive core measurements from sites 999 and 1001 in the Caribbean Sea: application to the late paleocene thermal maximum. In: Leckie, R.M., Sigurdsson, H., Acton, G.D., Draper, G. (Eds.), *Proceedings of the ODP, Scientific Results*, pp. 191–203.
- Sarnthein, M., Tetzlaff, G., Koopmann, B., Wolter, K., Pflaumann, U., 1981. Glacial and interglacial wind regimes over the eastern subtropical Atlantic and North-West Africa. *Nature* 293, 193–196.
- Sirocko, F., Sarnthein, M., Lange, H., Erlenkeuser, H., 1991. Atmospheric summer circulation and coastal upwelling in the Arabian Sea during the Holocene and the last glaciation. *Quat. Res.* 36, 72–93.
- Spooner, M.I., De Deckker, P., Barrows, T.T., Fifield, L.K., 2011. The behaviour of the Leeuwin Current offshore NW Australia during the last five glacial-interglacial cycles. *Glob. Planet. Change* 75, 119–132.
- Stuut, J.-B.W., Prins, M.A., Schneider, R.R., Weltje, G.J., Jansen, J.H.F., Postma, G., 2002. A 300-kyr record of aridity and wind strength in southwestern Africa: inferences from grain-size distributions of sediments on Walvis Ridge, SE Atlantic. *Mar. Geol.* 180, 221–233.
- Stuut, J.-B.W., Crosta, X., Van der Borg, K., Schneider, R.R., 2004. The relationship between Antarctic sea ice and South-western African climate during the Late Quaternary. *Geology* 32, 909–912.
- Stuut, J.-B.W., Lamy, F., 2004. Climate variability at the southern boundaries of the Namib (southwestern Africa) and Atacama (northern Chile) coastal deserts during the last 120,000 yr. *Quat. Res.* 62, 301–309.

- Stuut, J.-B.W., Zabel, M., Ratmeyer, V., Helmke, P., Schefuß, E., Lavik, G., Schneider, R.R., 2005. Provenance of present-day eolian dust collected off NW Africa. *J. Geophys. Res.* 110. <http://dx.doi.org/10.1029/2004JD005161>.
- Stuut, J.-B.W., Marchant, M., Kaiser, J., Lamy, F., Mohtadi, M., Romero, O., Hebbeln, D., 2006. The late Quaternary paleoenvironment of Chile as seen from marine archives. Special volume "The Andes: Past and present processes in an active margin orogen" *Geol. Helvetica* 61, 135–151.
- Stuut, J.-B.W., Kasten, S., Lamy, F., Hebbeln, D., 2007. Sources and modes of terrigenous sediment input to the Chilean continental slope. *Quat. Int.* 161, 67–76.
- Tachikawa, K., Cartapanis, O., Vidal, L., Beaufort, L., Barlyaeva, T., Bard, E., 2011. The precession phase of hydrological variability in the Western Pacific Warm Pool during the past 400 ka. *Quat. Sci. Rev.* 30, 3716–3727.
- Taylor, J.G., Pearce, A.F., 1999. Ningaloo Reef currents: implications for coral spawn dispersal, zooplankton and whale shark abundance. *J. R. Soc. West. Aust.* 82, 57–65.
- Thiede, J., 1979. Wind regimes over the Late Quaternary southwest Pacific Ocean. *Geology* 7, 259–262.
- Tjallingii, R., Röhl, U., Kölling, M., Bickert, T., 2007. Influence of the water content on X-ray fluorescence core-scanning measurements in soft marine sediments. *Geochem. Geophys. Geosystems* 8, Q02004.
- Tjallingii, R., Claussen, M., Stuut, J.-B.W., Fohlmeister, J., Jahn, A., Bickert, T., Lamy, F., Röhl, U., 2008. Coherent high- and low-latitude control of the northwest African hydrological balance. *Nat. Geosci.* 1, 670–675.
- Tjallingii, R., Statterger, K., Wetzel, A., Van Phach, P., 2010. Infilling and flooding of the Mekong River incised valley during deglacial sea-level rise. *Quat. Sci. Rev.* 29, 1432–1444.
- van der Kaars, S., De Deckker, P., 2002. A Late Quaternary pollen record from deep-sea core Fr10/95, GC17 offshore Cape Range Peninsula, northwestern Western Australia. *Rev. Palaeobot. Palynol.* 120, 17–39.
- van der Kaars, S., De Deckker, P., Gingele, F.X., 2006. A 100 000-year record of annual and seasonal rainfall and temperature for northwestern Australia based on a pollen record obtained offshore. *J. Quat. Sci.* 21, 879–889.
- Vörösmarty, C.J., Fekete, B.M., Meybeck, M., Lammers, R.B., 2000. Global system of rivers: its role in organizing continental land mass and defining land-to-ocean linkages. *Glob. Biogeochem. Cycles* 14, 599–621.
- Weltje, G., 1997. End-member modelling of compositional data: numerical-statistical algorithms for solving the explicit mixing problem. *J. Math. Geol.* 29, 503–549.
- Weltje, G.J., Prins, M.A., 2003. Muddled or mixed? Inferring palaeoclimate from size distributions of deep-sea clastics. *Sediment. Geol.* 162, 39–62.
- Weltje, G.J., Prins, M.A., 2007. Genetically meaningful decomposition of grain-size distributions. *Sediment. Geol.* 202, 409–424.
- Weltje, G.J., Tjallingii, R., 2008. Calibration of XRF core scanners for quantitative geochemical logging of sediment cores: theory and application. *Earth Planet. Sci. Lett.* 274, 423–438.
- Woo, M., Pattiaratchi, C., Schroeder, W., 2006. Dynamics of the Ningaloo current off Point Cloates, Western Australia. *Mar. Freshw. Res.* 57, 291–301.